FIRST SEMI-ANNUAL TECHNICAL PROGRESS REPORT
For Award Period 10/1/01 – 4/1/02

DoE Award #**DE-FC26-01NT41203**
"High-Efficiency Nitride-Based Solid-State Lighting"

APRIL 30, 2002

Authors: Dr. Paul T. Fini, Prof. Shuji Nakamura

University of California, Santa Barbara
Materials Dept., Bldg. 503 rm. 1355
Santa Barbara, CA 93106-5050

DISCLAIMER

ABSTRACT

In this semiannual report we summarize the progress obtained in the first six months with the support of DoE contract #**DE-FC26-01NT41203**, entitled "High-Efficiency Nitride-Based Solid-State Lighting". The two teams, from the University of California at Santa Barbara (Principle Investigator: Dr. Shuji Nakamura) and Rensselaer Polytechnic Institute (led by Dr. N. Narendran), are pursuing the goals of this contract from thin film growth, characterization, and packaging standpoints. The UCSB team has made significant progress in the development of GaN vertical cavity surface-emitting lasers (VCSELs) as well as light-emitting diodes (LEDs) with AlGaN active regions emitting in the ultraviolet (UV). The Rensselaer team has developed target specifications for some of the key parameters for the proposed solid-state lighting system, including a luminous flux requirement matrix for various lighting applications, optimal spectral power distributions, and the performance characteristics of currently available commercial LEDs for eventual comparisons to the devices developed in the scope of this project.

TABLE OF CONTENTS

LIST OF GRAPHICAL MATERIALS

Fig. 27. Laser pointer source model

Fig. 28. Line chart and raster chart for laser pointer source model

Fig. 29. Examples of conceptual designs for reflective, waveguide, and transmissive optical solutions for general illumination.

Fig. 30. Cylinder rod and square rod waveguide optics

Fig. 31. Transmissive optical model showing a picture of the model, a line chart and a raster chart of the illuminance

Fig. 32. RTIR study of the polymerization of PC1000 in the presence of SOC1O and in the presence and absence of 20% by weight of a poly(butyl methacrylate-methylmethacrylate) copolymer.

Fig. 33. Effect of the addition of 10% and 20% of Poly(BMA-co-MMA) on the polymerization of PC1000 with 1% and 2% of SOC10 as the photoinitiator.

Fig. 34. RTIR Comparison of the photopolymerization rates of PC1000 in the presence of poly(BMA-co-MMA) and with poly(EMA).

EXECUTIVE SUMMARY

Recently, solid-state lighting based on GaN semiconductors has made remarkable breakthroughs in efficiency. GaN-based light-emitting diodes (LEDs) emit bright blue and green light and complete the color spectrum, enabling a team lead by Dr. Shuji Nakamura (lead PI) to first successfully commercialize white LEDs in 1997 at Nichia Chemical Industries. With further improvements to GaN-based LEDs and laser diodes (also originally demonstrate by Nakamura and coworkers), we plan to achieve a solid-state light source with >50% efficiency (corresponding to a luminous efficiency of 200 lm/W). GaN LEDs already surpass incandescent technology and have the potential to displace halogen and fluorescent lighting. Not only would GaN-based lasers be the most efficient visible light sources, but they would be non-toxic (mercury and arsenic-free) and have projected lifetimes longer than 10 years.

We have assembled a team of researchers in the Materials Department at UC Santa Barbara and at the Lighting Research Center (LRC) at Rensselaer Polytechnic Institute to explore the fundamental issues associated with nitride-based solid-state lighting. The work at UCSB will focus on basic materials and device development. The work at RPI will focus on challenges in packaging, fixturing, testing, and evaluation of nitride-based solid-state lighting.

The ultimate goal at UCSB will be the demonstration of a white-light emitter based on a continuous-wave GaN-based vertical cavity surface emitting laser. Realization of such a structure will require continued improvements in all aspects of our materials. We will focus on the development of bulk GaN substrates which would enable back-side contacting, allow for improved cleaved laser facets (useful for our initial proposed work on edge-emitting lasers), provide improved thermal conduction over sapphire substrates, and have reduced threading dislocation densities. We will work to optimize all aspects of the growth structure with particular emphasis on improvement of InGaN quantum well growth and p-GaN layer growth. As a result of this work, we will demonstrate a nitride-based white light source with an efficiency of 200 lm/W. The goal for the LRC will be to utilize the GaN-based laser diode technology to create a light source/fixture useful for general lighting applications and quantify its merits with respect to traditional light sources.

To date, the UCSB team has made significant progress in the development of GaN vertical cavity surface-emitting lasers (VCSELs) as well as light-emitting diodes (LEDs) with AlGaN active regions emitting in the ultraviolet (UV). The Rensselaer team has developed target specifications for some of the key parameters for the proposed solid-state lighting system, including a luminous flux requirement matrix for various lighting applications, optimal spectral power distributions, and the performance characteristics of currently available commercial LEDs for eventual comparisons to the devices developed in the scope of this project.

EXPERIMENTAL

E.1 Vertical Cavity Surface Emitting Laser (VCSEL) Fabrication

Two approaches were explored in the VCSEL device design. In the first, the devices were fabricated using a two top contact scheme, with indium tin oxide (ITO) as the transparent p-contact. The ITO was deposited by DC magnetron sputtering in an oxygen ambient, then annealed at 500°C for 3 minutes to achieve transparency. An 11.5 period Ta_2O_5/SiO_2 dielectric mirror (R > 99.5%) was deposited at 250°C on the contacted side, followed by flip-chip bonding of the devices onto an AlN submount. The sapphire substrate was then removed via laser-assisted debonding. Finally, the now-upturned GaN:Si was polished and a second 11.5 period DBR was deposited to form a 6 um thick cavity.

In the second design, the samples were implanted with 180 keV aluminum ions in doses of 10^{13}, 10^{14}, and 10^{15} cm^{-2} prior to device fabrication, followed by a regrowth of 1230Å of GaN:Mg. The current confinement provided by the ion implantation allowed for the use of a ring-shaped ohmic metal p-contact (instead of ITO). Otherwise, the device fabrication remained the same.

Figure 1 presents a cross-section schematic of the ITO-contacted device structure, as well as an SEM micrograph of a diode just prior to flip-chip bonding. While the end design is somewhat different than traditional GaAs or InP based VCSELs (Fig. 1), the overall objective is the same: to minimize the losses in a cavity with a short gain medium so that the lasing threshold can be reached. This minimization is far more critical in a VCSEL as compared to an edge-emitting LD; Fig. 2 illustrates this point. The short amplification length (i.e. small per-pass gain) requires that losses such as transmission through the mirrors, absorption in contacts, and scattering from rough interfaces be much smaller than those tolerable in edge-emitting LDs. Of course the gain can be increased through higher current injection, but only to a point, after which heating effects dominate.

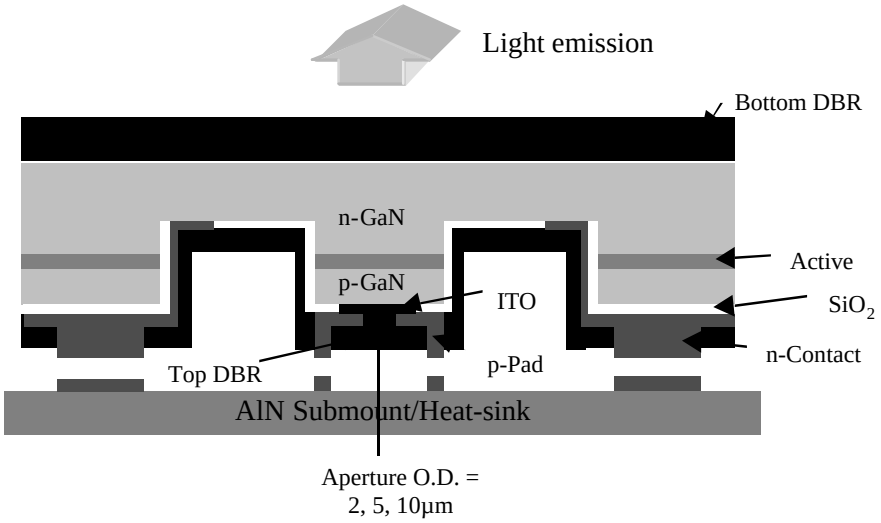

Fig. 1. Cross-section device schematic (above) and a SEM micrograph (below) of a 10 μm aperture device prior to flip-chip bonding.

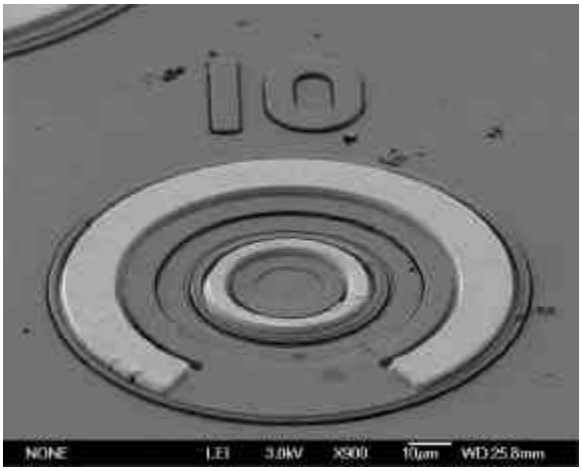

Fig. 1. (cont.)

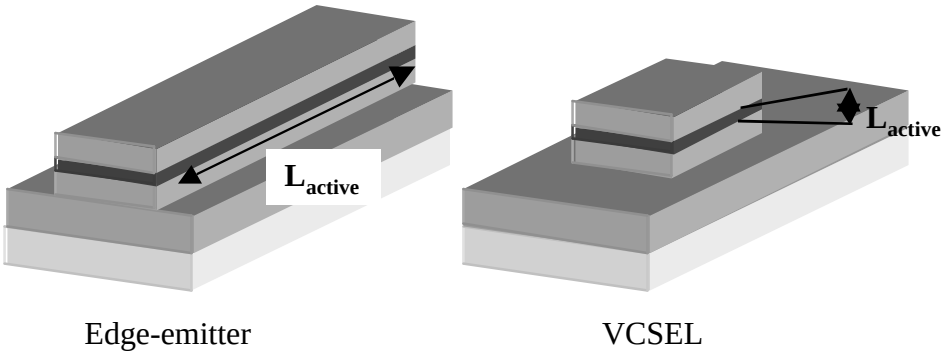

Fig. 2. Illustration of gain-length difference between edge-emitter and VCSEL.

Fig. 3 details the layer structure of the device presented in Fig. 1, grown by metalorganic chemical vapor deposition (MOCVD) on double-side polished sapphire substrates. Typically, the films consist of 5 μm of GaN:Si (with an optional insertion of 1000Å of InGaN:Si), five to ten 40Å $In_{0.1}Ga_{0.9}N$ wells separated by 80Å $In_{0.03}Ga_{0.97}N$:Si barriers, a 200Å $Al_{0.2}Ga_{0.8}N$ electron-barrier layer, and 5000Å of GaN:Mg.

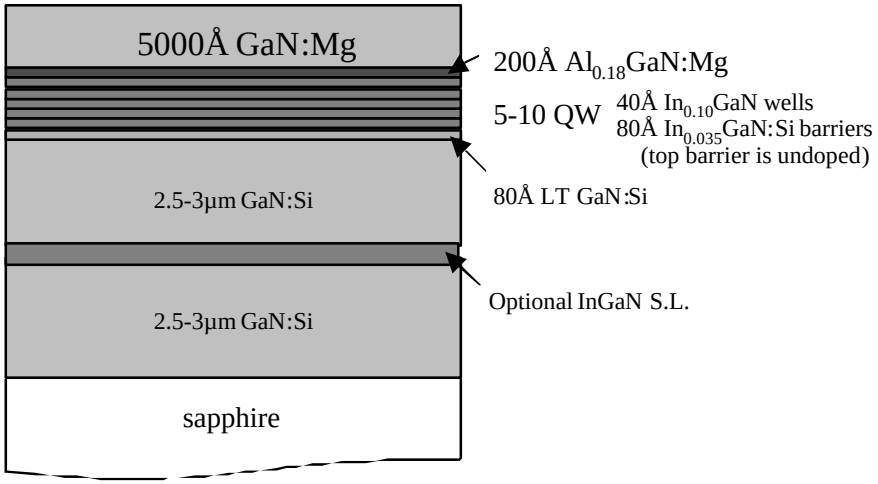

Fig. 3. MOCVD layer structure for the device in Fig. 1.

E.2 Ultraviolet LED Growth and Fabrication

In the development of an LED emitting at ~ 340nm (with the ultimate goal of laser emission at this wavelength), we have begun growth and fabrication of UV LEDs with $Al_xGa_{1-x}N$ active regions, where x is typically 10%. By immediately pursuing the more difficult goal of electrical pumping (vs. optical pumping), we hope to identify the key challenges to the development of an electrically pumped 340 nm laser. Specifically, our approach has been to deposit multi-quantum well (MQW) structures by Metalorganic Vapor Deposition (MOCVD) in a close-spaced showerhead reactor (Thomas Swan, Inc., Cambridge, UK). We have considered two structures: quantum wells with a 'bulk' AlGaN cladding, as well as short-period superlattice (SPASL) cladding. Both structures were grown on a ~ 2 µm GaN 'template' layer on 2" sapphire substrates. Schematics of both of these structures are shown below in Fig. 4. The active regions of the bulk-clad and SPASL-clad LEDs both had 3- and 5- period MQWs, which consisted of $Al_{0.07\text{-}0.08}GaN$ wells and $Al_{0.12}GaN$ barriers.

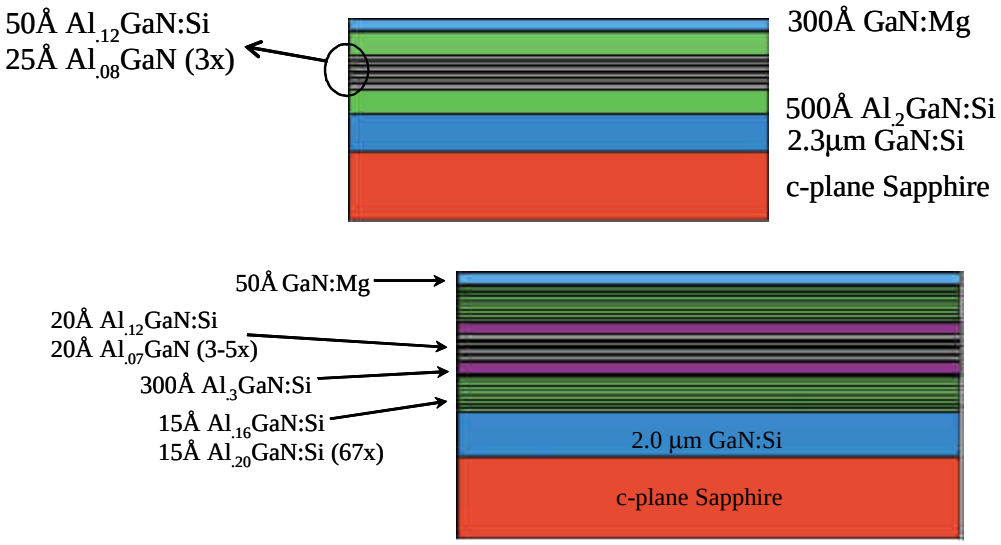

Fig 4. Schematics of the structures of UV LEDs with 'bulk' (top) and 'SPASL' (bottom) cladding layers.

Once grown, these films were processed into a 'conventional' LED test geometry by using chlorine Reactive Ion Etching (RIE) to define mesas. A dual top-contact scheme was used: Ti/Al/Ni/Au n-type contacts and Pd/Au p-type contacts were deposited by e-beam deposition. All intermediate steps were performed using conventional photolithography in our cleanroom.

Testing was performed in a direct-current (DC), un-pulsed mode up to a current of 100mA with a Hewlett-Packard 4145B Parameter analyzer. At present, this test equipment is limited to 100mA, so higher currents were not investigated. The light emitted from the **top** side of the devices was collected with a UV-enhanced photodiode located approximately 7mm above the wafer. The collection at this distance is about 20% of a total sphere. Spectra were obtained by coupling light into a fiber (located about 15mm above the sample) connected to a spectrometer.

E.3 Target Specifications for Solid-State Lighting System

Selecting target applications for a new light source depends on the amount of flux generated by the light source. Ultimately the solid-state sector of the lighting industry seeks to use LEDs for general illumination applications. The objective of this task is to create a matrix/guide to be used as a reference as to recommended lumens required for various applications. The format is intended to be clear, straightforward, and include criteria pertinent to specific tasks, such as CRI, CCT, dimmability, etc.

The task started off with a comprehensive literature search. The method used to formulate the matrix explained earlier was derived mostly from the Illuminating Engineering Society (IES) of North America recommendations for horizontal and vertical illuminance on task areas. Typical room dimensions were used to provide horizontal area in square feet, and typical ceiling heights were used to provide wall area in square feet to calculate vertical lumens. Once room dimensions were established, concepts for the various spaces were developed, which included typical luminaire placement to deliver general lighting as well as lighting to the task was inserted.

The areas selected represent a cross section of residential, retail/commercial and industrial spaces, and the guide will be separated accordingly. Each section will be divided into smaller task areas as per the following examples:

E.4 Optimum Spectral Power Distribution

Developing a light source and achieving high level of market penetration depends on how well human subjects like the quality of the light produced by this new source. The spectral power distribution (SPD) is an important parameter that makes a light source acceptable. In addition SPD determines the CRI, CCT, and luminous efficacy of the light source. Therefore, the objective of this task is to develop an optimal SPD for the target light source.

A human factors experiment was conducted to determine the optimum SPD. In an earlier study the LRC investigated the color rendering properties of several types of white LED reading lights and compared them to conventional halogen and incandescent reading lights (Narendran, 2002). In this earlier study human subjects viewed two identical scenes lit by different light sources and placed side by side. The human subject rated their preference for a given scene compared to the reference scene. The experimental setup is shown in Fig. 5.

Fig. 5. Front view of experimental apparatus

Each cabinet measured 15 inches by 15 inches. The interior of the cabinets was painted with matte finish white paint to ensure good mixing of light and uniform illuminance on the target surface. The light sources were mounted at the top of the cabinets inside a domed area pointing upwards. The light reached the displayed objects after bouncing off the ceiling area and the walls. As shown in Fig. 5, a color magazine, two soda cans (Pepsi® and Mountain Dew®), and a text card with various font sizes were placed inside the viewing area of the cabinets. Precautions were taken to ensure that the two cabinets were identical. A forehead holder was fixed in the middle frame of the apparatus to make sure that the subjects kept a consistent reading distance (20'') from the scene. Six different reading lights were evaluated against a standard halogen reading light. They included:

- Two red, green, blue (R,G,B) mix LED (one had high CRI, and the other low CRI);
- Three phosphor-based white LED systems (one was a single phosphor, second was a phosphor combined with amber, and third was a two phosphor high power LED);
- One incandescent light.

E.5 Commercial LED Product Evaluations

In order to benchmark performance and to identify the industry's state-of-the-art LEDs, the LRC is planning on testing high-power "illuminator" LED products. Presently LumiLeds Lighting and Optotechnologies offer high power LEDs suitable for illumination applications. Nichia Chemical (Japan) recently announced that they would be releasing a high power white LED (20 lumens, 23 lumens per watt). In the proposed test we hope to test the following LEDs:

LumiLeds:
Red, Green, Blue, and White Luxeon LEDs, both 1watt and 5-watts

Optotechnologies:
White, Shark devices

Nichia Chemicals:
White high-power LEDs

Products from Nichia may not be available till the end of 2002, and will be tested once they are in the market. In general, system integrators package these LED arrays differently and they may chose to drive them differently. Therefore, the proposed test will evaluate the above-mentioned products at two different temperatures and two different operating currents.

E.6 Development of Optical Designs For Next-generation Solid-State Lighting Fixtures

There are a number of steps involved to meet this objective. First, a literature search is done in order to determine what has been published on solid-state lighting for general illumination. Second, a typical lighting application must be selected and performance criteria determined. Third, optical modeling and testing of various laser diode sources is needed. Fourth, a number of conceptual ideas must be modeled optically to determine their performance. Fifth, a design path must be selected and specified to build and test the source/optic combination. Finally, a mock-up of a typical lighting application must be built and measurements must be taken to determine how well the measurements meet the design values.

The lighting application that was selected is a conference room that is 10' x 10' x 9'. The Recommended Practice for Office Lighting (ANSI/IESNA RP-1-1993) recommends:

1. For a combination of paper and screen-based tasks, provide a maximum of 50 fc (500lx) of general lighting on the work plane.
2. Lower general illuminances may be appropriate if tasks are primarily screen-based, or if paper task illuminances are supplemented with task lighting.
3. For a direct lighting system, select luminaires that do not exceed 850 cd/m2 at 65°, 350 cd/m2 at 75°, 175 cd/m2 at 85°.
4. For an indirect lighting system, select luminaries that limit maximum ceiling luminance to 850 cd/m2 or less.
5. The luminance ratios between paper and remote light surfaces should not exceed 1:10 or 10:1.

The mock-up of this lighting application will be a 1/10th scale model, or a 1' x 1' x 0.8' conference room. Multiple distribution types such as direct, semi direct, and indirect distributions, and fixture positions were analyzed for a conference room of size 10' X 10' X 8', to identify the best distribution type to obtain illuminance levels for the task. This analysis was done using Lightscape software.

E.7 Development of suitable epoxy materials for packaging solid-state devices

There are three advances in chemistry developed by our group that are of interest for the fabrication of LED encapsulants. The first is the development of highly reactive siloxane epoxides. The monomer and oligomer with structures shown below are highly reactive and have some resemblance to glass that is the "ideal" encapsulant.

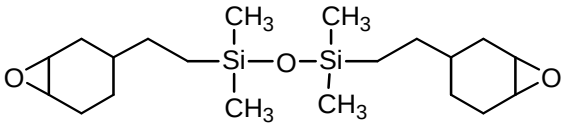

PC1000

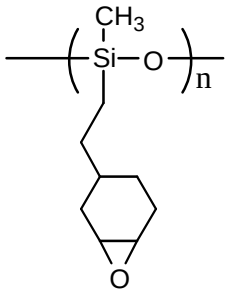

PC2003

These materials undergo facile curing when exposed to light and/or heat in the presence of an onium salt photoinitiator to give highly crosslinked network structures. The onium salt initiators were developed in this laboratory and have become commercially available for use in coatings, adhesives and printing inks. An example of an onium salt photoinitiator is the triarylsulfonium salt with the structure shown below.

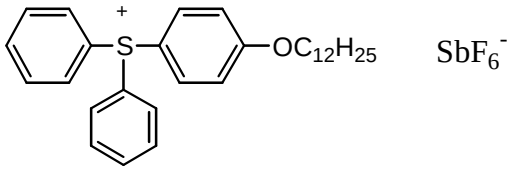

SOC12

The use of onium salts together with the above epoxide monomers and also biscycloaliphatic epoxy monomers such as ERL-4221E from Union Carbide/Dow Chemical gives cured resins with a polyether structure rather than the ester-alcohol structure obtained by conventional epoxide-anhydride

curing systems. These materials would be expected to display better photo- and thermal-oxidative resistance.

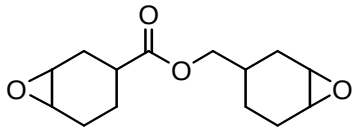

ERL-4221E

However, some problems may be encountered with the photopolymerization of these monomers. For example, the high shrinkage that occurs during polymerization may result in cracking of the encapsulant or loss of adhesion at the die surface. More seriously, the shrinkage may put stress on the wire bonds to the dies. In addition, the viscosity of these monomers is too low for them to be used as encapsulants. We have now observed that the epoxy monomers and oligomers shown above are excellent solvents for a variety of high polymers such as poly(methylmethacrylate) with good light resistance characteristics. Viscous solutions are formed in which it is possible to dissolve photoinitiators like IOC10 (1-2% is required in the formulations). These solutions are ideally suited for encapsulants. Through the addition of these polymers we hope to alleviate the problems cited above by reducing shrinkage and increasing flexibility. The viscosity of these mixtures can be adjusted within wide tolerances. This permits the formulation of materials with sufficient viscosity to flow and cover the semiconductor dies but also with some thixotropy so that the materials remain where the are placed during encapsulation.

It was of primary concern with these new mixtures of epoxy monomers with various polymers to determine whether the epoxy curing reaction could be carried out in a similar manner as when no polymer additives are added. Preliminary studies have shown definitively that this is indeed the case. Kinetic studies were carried out using Real-time infrared spectroscopy (RTIR). Using this technique we are able to follow the course of the very rapid polymerization in real time while simultaneously irradiating the sample with UV light.

RESULTS AND DISCUSSION

R.1 VCSEL Development

The completed VCSEL devices were pulse-tested at room temperature, applying voltage pulses ranging from 50 to 500 nsec at both 5 and 10 kHz. A HP 8114A pulse generator was used as the injection source. Light emission from the devices was uniform over the aperture area, indicative of current spreading by the ITO contact. A 100 μm diameter multimode fiber-optic probe was used to collect and guide the light into a Hamamatsu photomultiplier tube (PMT), biased at 900-1200 V.

Light output versus current (L-I) and current-voltage curves (I-V) for a 10 quantum well (QW), 10 μm diameter aperture device with an ITO contact are shown in Fig. 6 for varying pulse lengths.

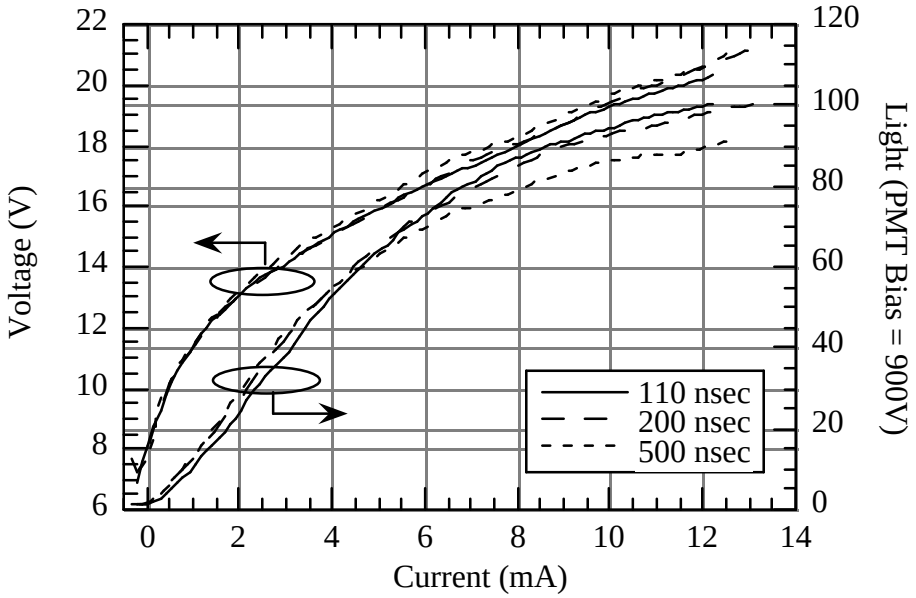

Fig.6. L-I-V characteristics for a 10 μm aperture 10 QW device with an ITO contact, pulsed at 5 kHz with varying pulse widths.

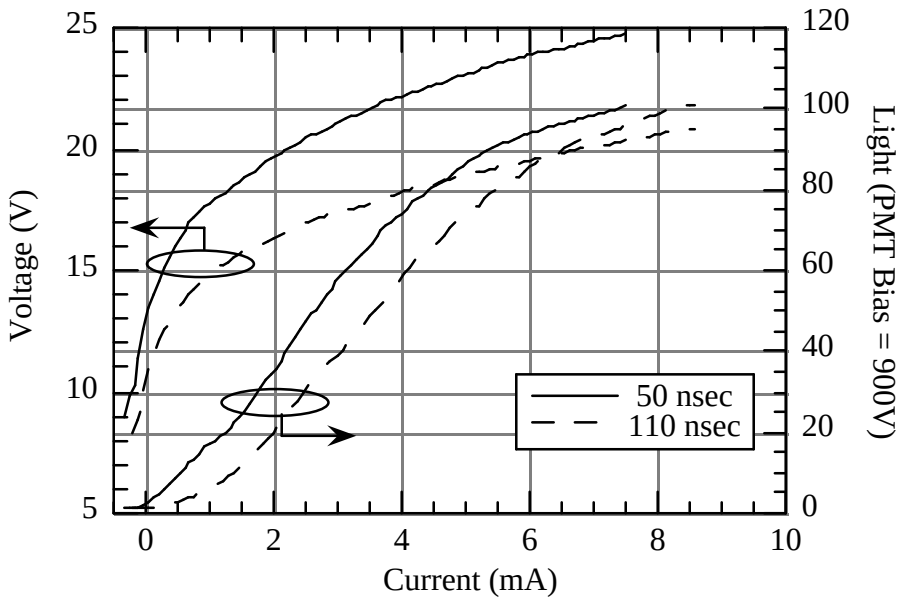

Fig.7. L-I-V characteristics for a 10 μm aperture 10 QW device with an ITO contact, pulsed at 5 kHz.

The turn-on voltage that is a result of the Schottky ITO contact is approximately 12–15 V, although higher at 50 nsec pulse lengths (Fig. 7). The L-I characteristics tail off at higher current densities indicating that the devices are heating up during the pulse. As expected, this tail-off occurs at lower currents for longer pulses. A slight bend in the L-I at low currents (< 2 mA) is probably indicative of non-radiative trap saturation. Reducing the number of QWs from 10 to 5 did not significantly alter device performance (Fig. 8).

Radiative performance scaled with aperture size, although I-V characteristics did not (Fig. 9). Smaller devices seemed to handle much larger current densities (up to 220 kA/cm^2) than those with larger ITO apertures, before catastrophically short circuiting – somewhat surprising considering that heating is inversely proportional to the device size. For VCSEL-type geometries, the relation between change in temperature and power dissipation is,

$$\Delta T = P_D Z_T = P_D \frac{1}{2xs}, \qquad (1)$$

where s is the diameter of the device is and ξ is the thermal conductivity (ξ_{GaN} = 1.3 W/cmK). A possible explanation is that shorting occurs along threading dislocations; smaller devices have fewer of these conduction paths.

As an aside, the light output scale is listed in arbitrary units primarily due to uncertainty in the collection efficiency of the fiber probe. The measurement is in reality a voltage taken from the peak of the PMT signal on the oscilloscope. Assuming no loss in the fiber – at the device, along the fiber, and at the PMT – 1 volt on the readout translates to approximately 2 nW of output power, after accounting for the responsivity of the PMT and a gain of 1.1x10^6.

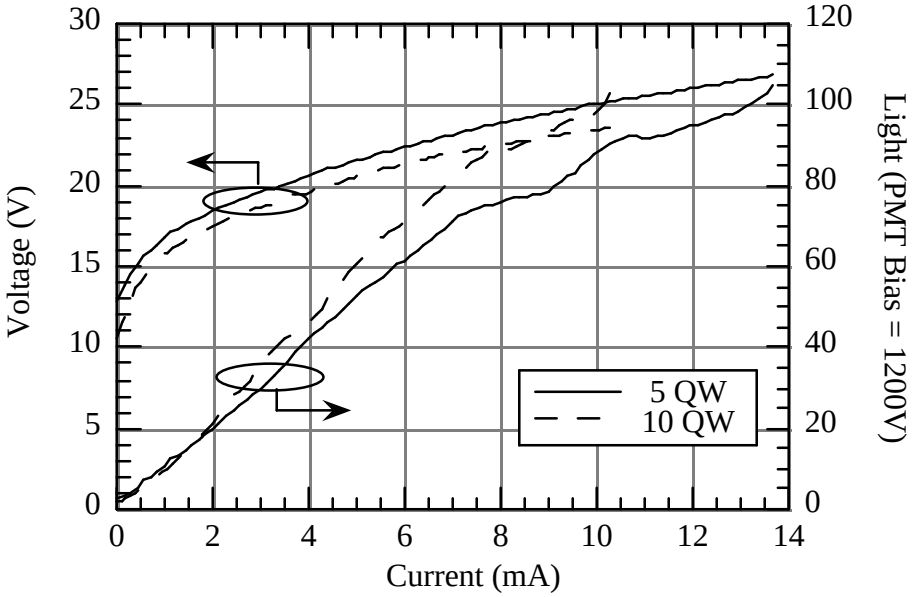

Fig. 8. Comparison of 110 nsec, 5 kHz pulsed L-I-V curves for 5 and 10 QW 2 μm aperture devices with ITO contacts.

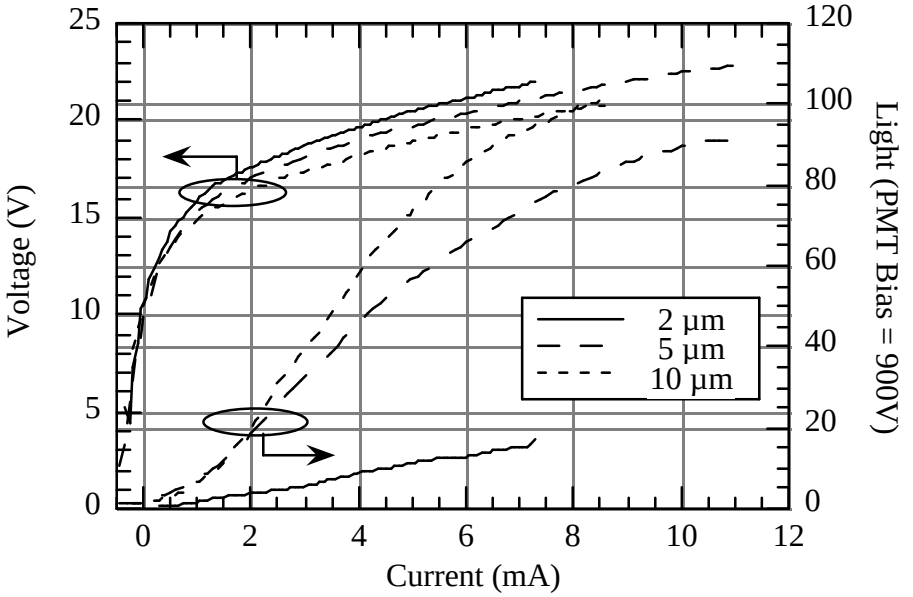

Fig. 9. Comparison of 110 nsec, 5 kHz pulsed L-I-V curves for 10 QW devices with ITO contacts and varying aperture diameters.

Devices with a 5 μm diameter implant-defined aperture were also tested, and the L-I-V characteristics are shown in Fig. 10. Due to unoptimized regrowth conditions the turn-on voltage of these devices is still around 15 V, even though the devices incorporate 2 ohmic metal contacts. The bend in the L-I curves of these diodes at low currents is more significantly pronounced than for the ITO-devices, indicating a greater presence of non-radiative traps.

Emission from the devices was centered between 400 and 410 nm. A pulsed spectrum for a 10 μm aperture device is shown in Fig. 11, taken with a CVI SM240 integrating diode array spectrometer. Cavity modes are clearly present and spaced 4 to 5 nm apart, as expected for a cavity length of approximately 5.5 μm. The spectral linewidth of the modes is around 0.8 nm full width at half

maximum (FWHM), from which we calculate a cavity Q of >510. Two other peaks of note are visible in the spectrum.

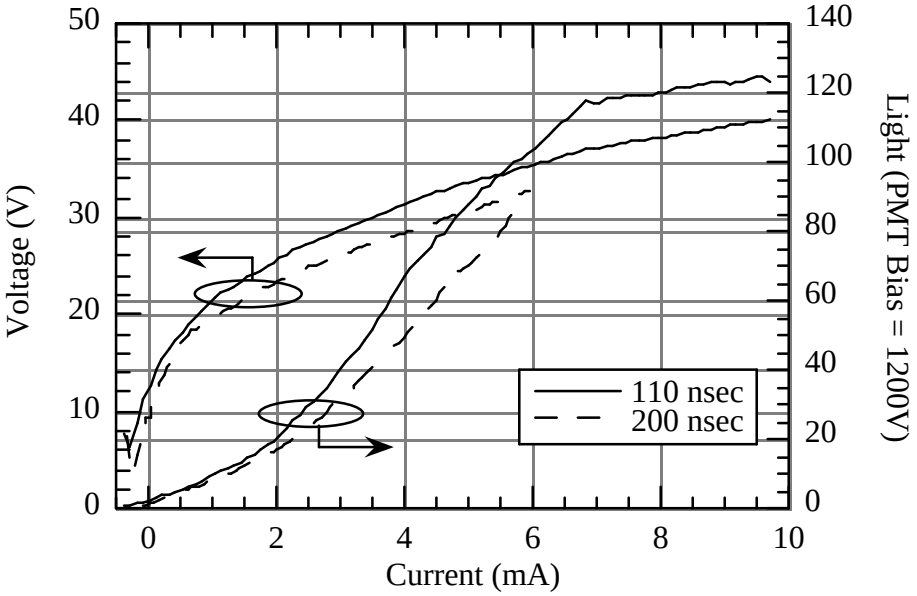

Fig. 10. L-I-V characteristics of a 5 μm implant-defined aperture device, pulsed at 5 kHz and varying pulse widths.

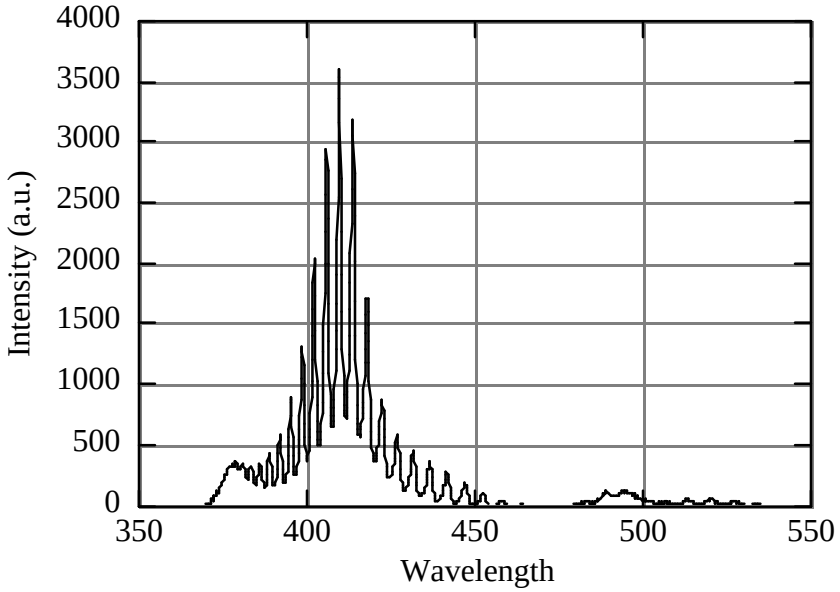

Fig. 11. Pulsed spectrum (200 nsec, 5 kHz) for a 10 μm aperture 10 QW device with an ITO contact.

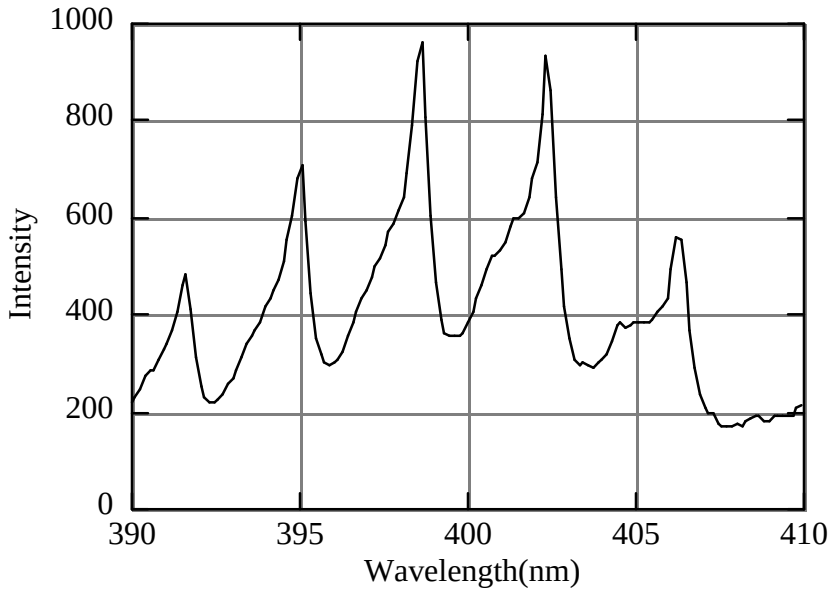

Fig. 12. Zoomed-in pulsed spectrum (50 nsec, 5 kHz) for a 10 μm aperture 10 QW device with an ITO contact.

The first is a low-intensity peak at around 500 nm. We believe this to be a result of constructive interference with an air-gap cavity formed between the AlN submount and the first dielectric DBR. The second peak, at a shorter wavelength emission of approximately 380 nm – corresponding to the InGaN barriers – appears at higher current densities for some devices. This peak increases in intensity with higher current injection while the intensity of the primary peak at 400 nm saturates. Most likely this is carrier leakage due to heating, corresponding to the roll-off in the L-I characteristics at higher currents.

There were slight variations between devices. Fig. 12 shows a pulsed spectrum for another diode from the same wafer. The modal linewidth in this case is around 0.6 nm (Q >660). Of interest is the appearance of secondary shoulder peaks at the left (shorter wavelength) of the main modes, also evenly spaced. These may be lateral modes, reflecting off of the dielectric layers defining the device aperture.

R.2 UV LEDs

The room-temperature photoluminescence spectra of UV LEDs with 'bulk' cladding, 2.5 nm $Al_{.06}GaN$ quantum wells, and varying amounts of Al in the 5.0 nm quantum well barriers are shown in Fig. 13 below. Strong emission was detected at ~ 345nm (QW emission) and ~365nm (the GaN band edge) for all structures. The GaN band-edge emission came from the underlying GaN 'template' layer, which is absorbing at the QW emission wavelength, but had much lower dislocation density than an AlGaN template layer of the same thickness. As the amount of Al in the AlGaN barriers between QWs was increased, the intensity of the QW emission decreased, which we believe is due to higher strain-driven piezoelectric fields in the wells. These strong fields tend to spatially separate electrons and holes and therefore reduce recombination efficiency, a well-known effect called the Quantum-confined Stark Effect.

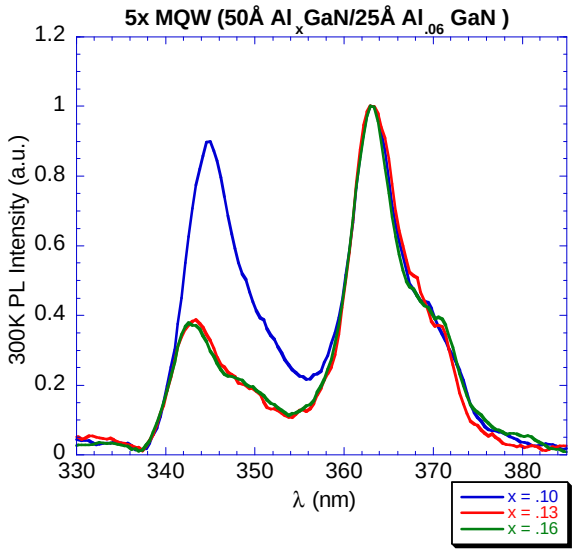

Fig. 13. Photoluminescence of bulk-clad LEDs with varying amounts of Al in the barriers between quantum wells.

As mentioned in the previous section, in addition to 'bulk' AlGaN cladding layers, we also investigated the use of AlGaN superlattices. In preparation for electroluminescence measurements, the electrical properties of processed device structures were first measured, the results of which are shown in Fig. 14. Although all devices had a turn-on voltage of approximately three volts, it became immediately apparent that LEDs with SL cladding layers had lower series resistance, as indicated by their higher I-V curve slopes. This was due to higher hole generation in such SLs, which our group has exploited in the past – a hole concentration enhancement of over 10 times has been observed. The band bending between alternating layers in these SLs causes more Mg acceptor atoms to be ionized, leading to hole accumulation in 'sheets' at the SL interfaces.

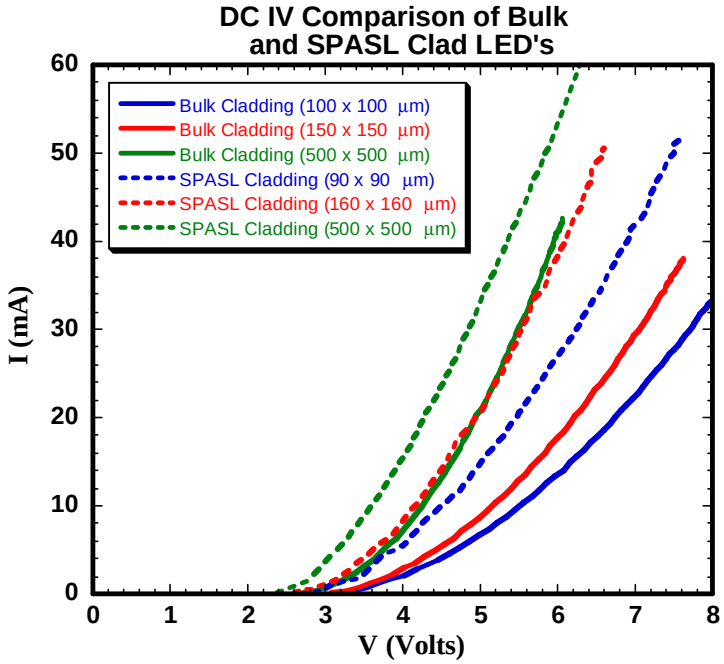

Fig. 14. Comparison of DC IV for bulk- and SPASL-clad MQW UV LEDs.

After initial I-V measurements were completed, electroluminescence (EL) spectra were recorded for SL-clad LEDs at various pump currents. In Fig. 15, EL from 130µm x 130µm LEDs with three

QWs as well as five QWs is plotted vs. wavelength. For each drive current, the EL intensity at 348 nm increased as the number of QWs was increased. The higher EL intensity with five QWs shows there was effective pumping of all of the wells despite the low hole mobility typically seen in AlGaN ternary alloys. In the future, we will fabricate LEDs with higher numbers of QWs to see when this trend ceases, which is expected to occur when holes are no longer able to diffuse to those QWs closest to the n-type side of the device.

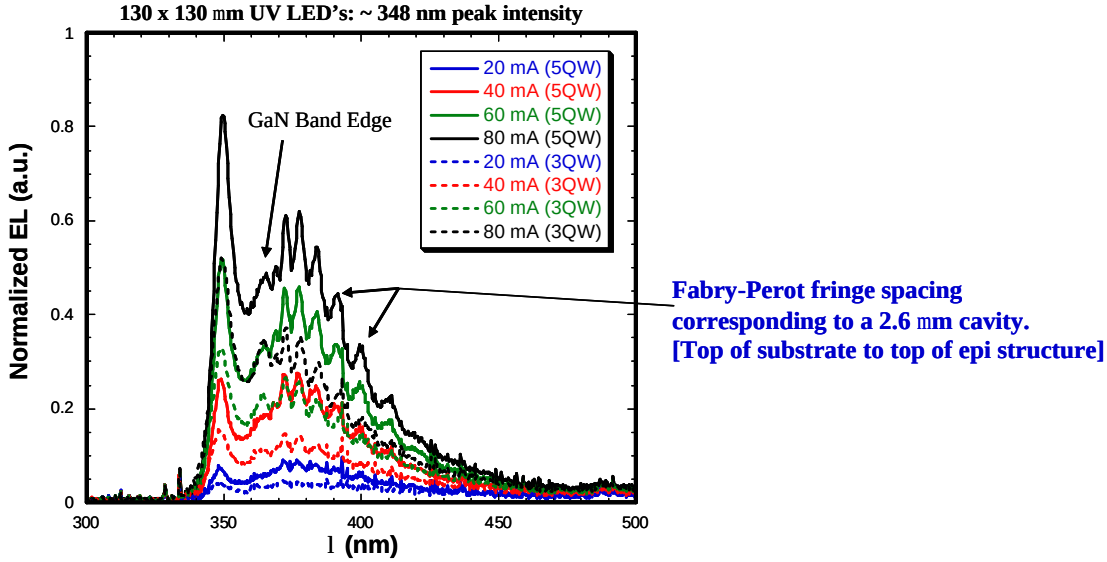

Fig. 15. Electroluminescence (EL) from SPASL-clad 130x130 μm UV LEDs with 3 and 5 QWs, at 20, 40, 60, and 80 mA drive current.

In comparing SL-clad LEDs with three and five QWs, we measured the dependence of both voltage and output power (at 348 nm) on input current, the results of which are shown in Fig. 16. For each number of QWs, we also fabricated devices of two sizes. As expected, the output power of the smaller (130 x 130 μm) devices was higher throughout the input current range, since the current density in these devices was also higher. However, the voltage for smaller devices was in general slightly higher than for larger ones, which suggests problems with lateral p-type conductivity in these structures.

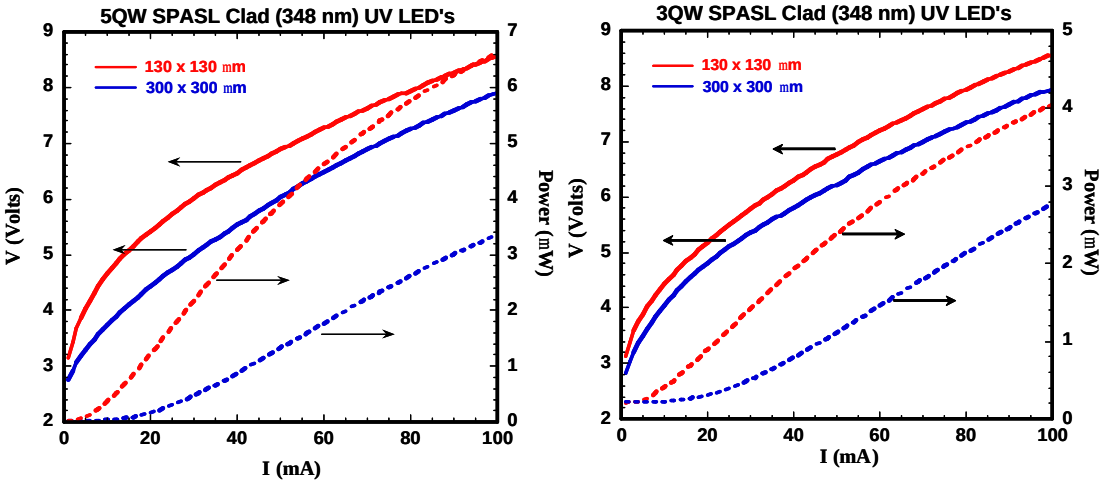

Fig. 16. Voltage (V) and output power (P) vs. current (I) for 5 QW vs. 3 QW SL-clad LEDs.

Finally, we compared the output power vs. current behavior of LEDs of various sizes. As the device size becomes smaller, the current density at a given nominal drive current is higher, which explains the difference between most of the curves in Fig. 17 below. However, at the highest current density (in the 130 x 130 μm device), the effects of device heating are evident, in particular since we

grew these structures on sapphire substrates. Sapphire has a low thermal conductivity compared to SiC and Si, and to (Al)GaN itself. In the future when we wish to test at higher current densities (for lasers in particular), heat sinking techniques will be necessary for devices on sapphire.

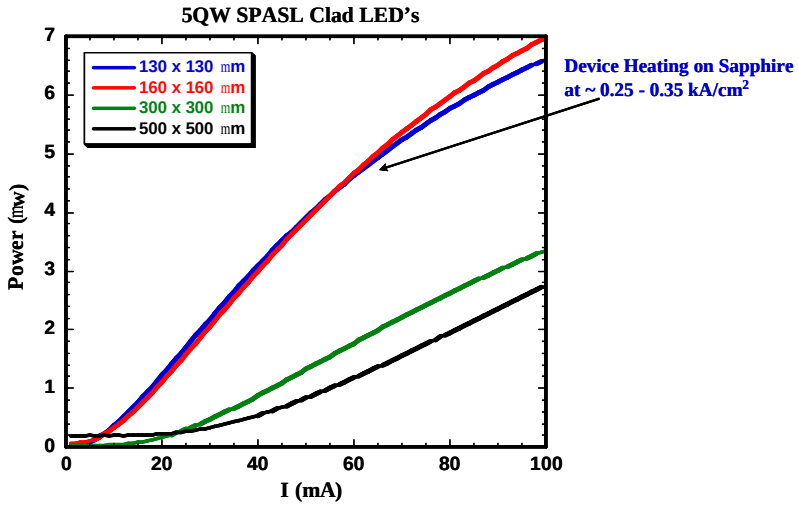

Fig. 17. Output power vs. current (I) for 5QW LEDs of various lateral sizes.

R.3 Target Specifications for Solid-State Lighting System

A worksheet was developed to calculate a basic lumen amount, which derived from the area of the room x the horizontal foot-candles plus the area of the walls x the vertical foot-candles (see Fig. 18). From those calculations, the individual rooms were then designed to include typical luminaries in general circulation areas, and on task areas, number and wattages. Figure 19 and Tables 1-4 illustrate the results to date, including, graph illustrating lumen ranges for tasks in that space, and tables showing other criteria important to the different tasks.

C1 = Task

A	B	C	D	E	F	G	H	I	J	K	L
Category	**Room**	**Task**	**Illumination Level (Hor)**	**Illumination Level (Vertical)**	**Dimension (Length)**	**Dimension (Width)**	**Ceiling Height**	**Area**	**Lumen (Hor)**	**Lumen (Ver)**	**Lumen**
Residential			lux	lux							
	Foyer		30	30	6	10	8	60	1800	1440	3240
	Kitchen		300	50	10	12	8	120	36000	4000	40000
	Dining Room		50		10	14	8	140	7000	80	7080
	Living Room		30	30	12	15	8	180	5400	2880	8280
	Bathroom		300	50	8	6	8	48	14400	3200	17600
	Bedroom		100		12	16	8	192	19200	96	19296
	Garage		10	5	12	20	8	240	2400	480	2880
	Storage		50	30	10	10	8	100	5000	2400	7400
		Dining	50		7	9	8	63	3150	56	3206
		Counters - Cutting	500	100	3	1.5	8	4.5	2250	2400	4650
		Critical Prep	500	100	3	1.5	8	4.5	2250	2400	4650
		Range	500	100	2	2	8	4	2000	1600	3600
		Sink	500	100	2	1.5	8	3	1500	1600	3100
		Pantry	300	30	6	4	8	24	7200	1440	8640
		Reading (Casual)	300	50	1.5	1.5	8	2.25	675	600	1275
		Reading (Seating)	300	50	1.5	1.5	8	2.25	675	600	1275
		Vanity	300	50	3	2	8	6	1800	1200	3000
		Dressing	300	50	8	4	8	32	9600	3200	12800
		Toilet	100	30	5	5	8	25	2500	1200	3700
		Filing	500	100	3	3	8	9	4500	2400	6900
		Music	500	30	6	2	8	12	6000	1440	7440
		Closet	50	30	5	5	8	25	1250	1200	2450

Fig. 18. Sample Worksheet Residential: Category/Room/Task

[Flux (lumens) = Area x Illuminance (fc)]

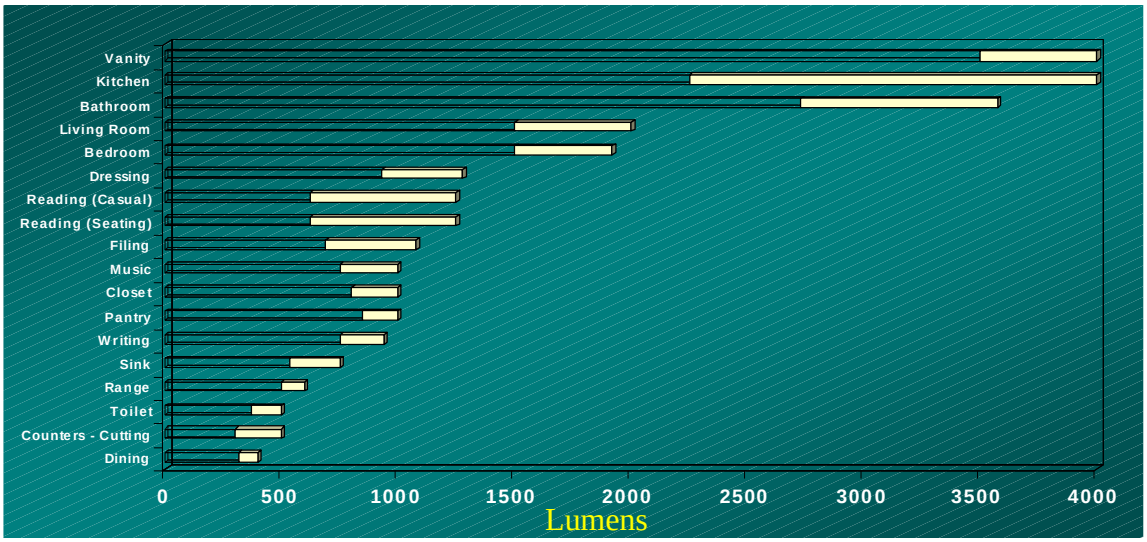

Fig. 19. Graphical illustration of lumen matrix

Table 1. Lighting specifications for an average residential kitchen

Space	Lumens (Lower range)	Lumens (Upper range)	Difference	Light Source	Efficacy	CRI	CCT
Kitchen	2250	4000	1750	(3) 60W - Incandescent A-lamp	12.5 l/W	>80	2800 - 4200
Pantry	845	1000	155	13W - CFL	65 - 70 l/W	>75	3200 - 4200
Sink	540	750	210	50W - Incandescent PAR-lamp	15 l/W	NA	2800 - 4500
Range	500	600	100	40W Appliance Lamp	12.5 l/W	>90	NA
Counters - Cutting	300	500	200	T-5 Linear fluorescent	40 l/W	>75	3000 - 6500
Dining	315	400	85	40W - Incandescent A-lamp	12.5 l/W	>90	2800 - 3500

Table 2. Lighting specifications for an average residential bedroom

Space	Lumens (Lower range)	Lumens (Upper range)	Difference	Light Source	Efficacy	CRI	CCT
Bedroom	1500	1920	420	(2) 60W Incandescent A-lamp	12.5 l/W	>75	2800 - 3500
Dressing	930	1280	350	75W Incandescent PAR-lamp	12.5 l/W	>80	3000 - 4000
Reading (Casual)	625	1250	625	50 - 100W Incandescent A-lamp	12.5 l/W	>80	3000 - 4500
Closet	800	1000	200	13W CFL	65 - 70 l/W	>80	3000 - 4500
Writing	750	940	190	60-75W Incandescent A-lamp	12.5 l/W	NA	NA

Table 3. Lighting specifications for an average residential living room

Space	Lumens (Lower range)	Lumens (Upper range)	Difference	Light Source	Efficacy	CRI	CCT
Living Room	1500	2000	500	(2) 50W - Incandescent PAR-lamp	15 l/W	>80	2800 - 3500
Reading (Seating)	625	1250	625	50 - 100W Incandescent A-lamp	12.5 l/W	>80	3000 - 4500
Filing	690	1080	390	Halogen Strip Light	15 l/W	NA	NA
Music	750	1000	250	50W - Incandescent PAR-lamp	15 l/W	NA	2800 - 4000

Table 4. Lighting specifications for an average residential bathroom

Space	Lumens (Lower range)	Lumens (Upper range)	Difference	Light Source	Efficacy	CRI	CCT
Vanity	3500	4000	500	(2) 25W T-8 Linear Fluorescent	80 l/W	>86	3200 - 4500
Bathroom	2730	3575	845	55W CFL	65 - 70 l/w	>70	3000 - 4000
Toilet	370	500	130	40W - Incandescent A-lamp	12.5 l/W	NA	2800 - 4500

The work in progress will continue to develop specifications for retail/commercial and industrial spaces. This task is estimated to be completed by the end of July 2002.

R.4 Optimum Spectral Power Distribution

The various light sources described in the Experimental section were evaluated against a standard halogen reading light. The evaluations indicated that although the high power two-phosphor LED based reading lights showed a high percentage acceptance in terms of general preference of an object's color appearance, the subjects' rating for the appearance of human skin tones was poor. The skin tone preference rating was worse for the single phosphor white LED. It was speculated that the deficiency of red in the phosphor white LED spectrum could be the reason for their poor color rendition of human skin tones. Therefore, by adding some red components into the high power LED spectrum, one can improve its color rending properties on human skin tones while preserving its excellent color rending properties on the other objects.

- Figure 20 shows the SPD of the high power LED.
- Figure 21 shows the improvement option 1: the high power LED mixed with 525nm green LED and 620nm red LED.
- Figure 22 shows the improvement option 2: the high power LED mixes with 525nm green LED and 640nm red LED.

The extra green was used to bring the mixed light source chromaticity coordinates back to the blackbody locus so that it exhibits a white appearance.

Similar to an earlier study, a human factors experiment was conducted to evaluated the above three light sources together with a halogen light source and the two RGB mix LED light sources used in the earlier study. Table 5 summarizes the characteristics of the six new experimental light sources. In this study, human subjects viewed two identical scenes placed side-by-side and lit by the six different light sources. Human subjects rated their preference for a given scene compared to the reference scene. 20 subjects were employed for this study. Figures 23 and 24 illustrate the experimental results from side

by side comparisons. Tables 5 and 6 summarize the individual subject rating results. A two-tailed Bonferroni paired t-statistic (P value = 0.05) is used for the data analysis. In Table 6, *** represents a statistically significant difference after Bonferroni correction and * represents a P value of 0.05 statistic without Bonferroni correction. From the results we have reached the following preliminary conclusions:

- Adding the red and green components into the high power LED spectrum, improved its color rending properties on human skin tones while preserving its excellent color rending properties on the other objects.
- There is no significant performance difference between the high power LED + 525nm green LED + 620nm red LED light source and the high power LED + 525nm green LED + 640nm red LED light source.
- In terms of skin tone preference, the two RGB-Mix LED reading lights still performed better than all other light sources evaluated in this study.

The work in progress will continue until the final analysis is completed and a recommendation is reached for identifying an optimum spectrum. This task is estimated to be completed by the end of June 2002.

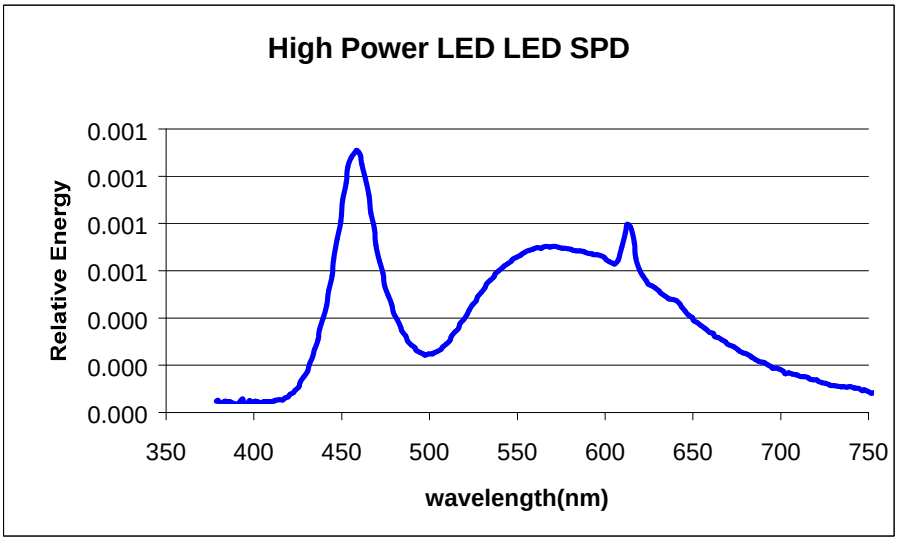

Fig. 20. High-Power LED SPD

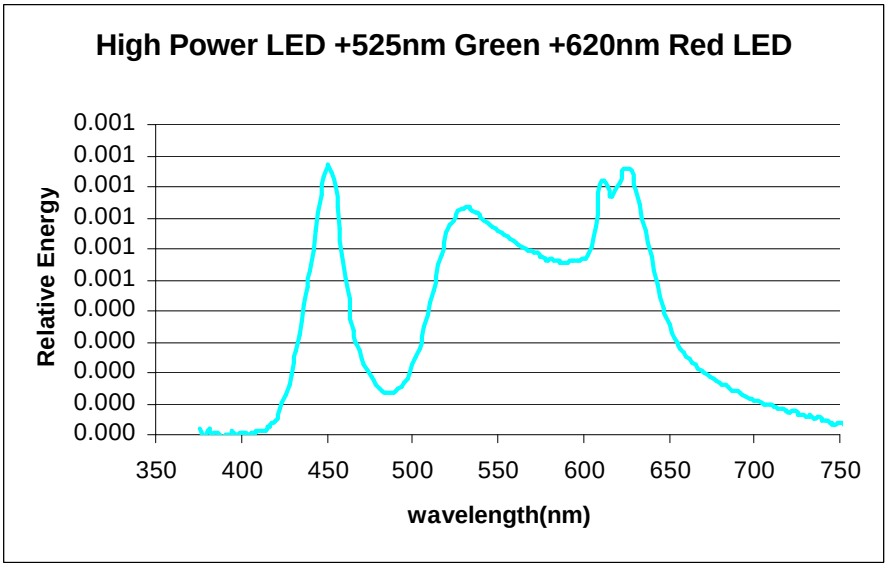

Fig. 21. High-Power LED blend, with 525nm Green LED and 620nm Red LED

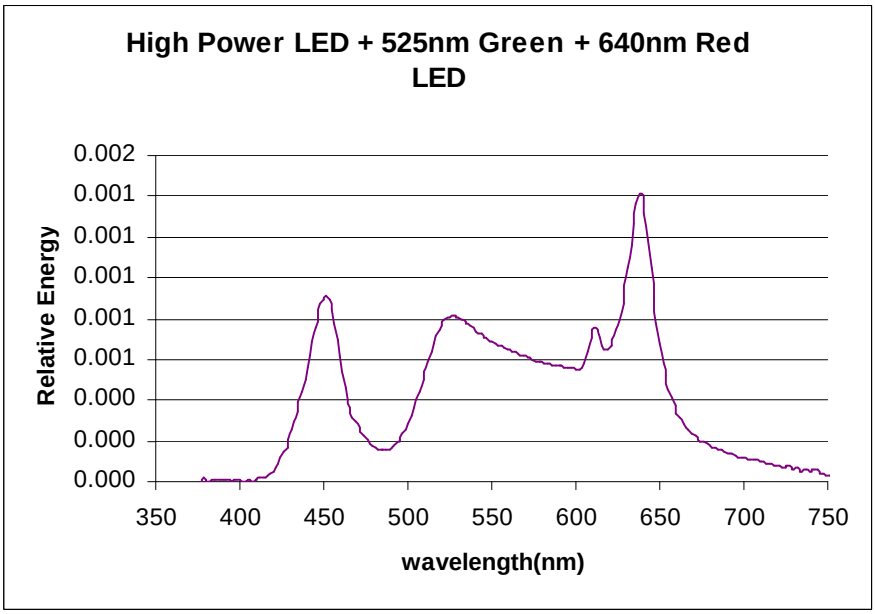

Fig. 22. High Power LED blend with 525nm Green LED and 640nm Red LED

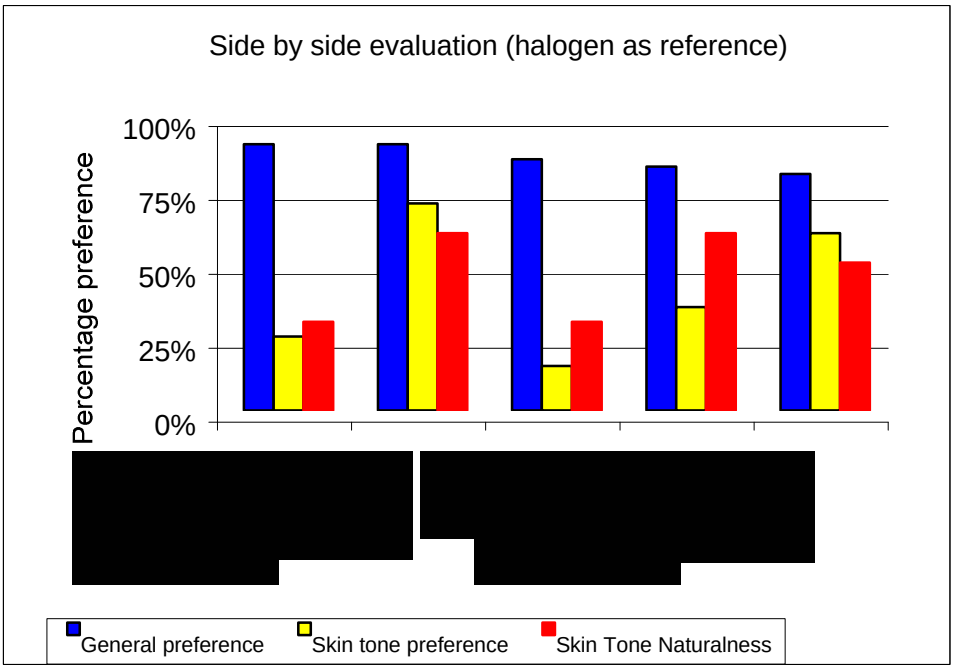

Fig. 23. Side-by-side Comparison with Halogen Reference Light Source

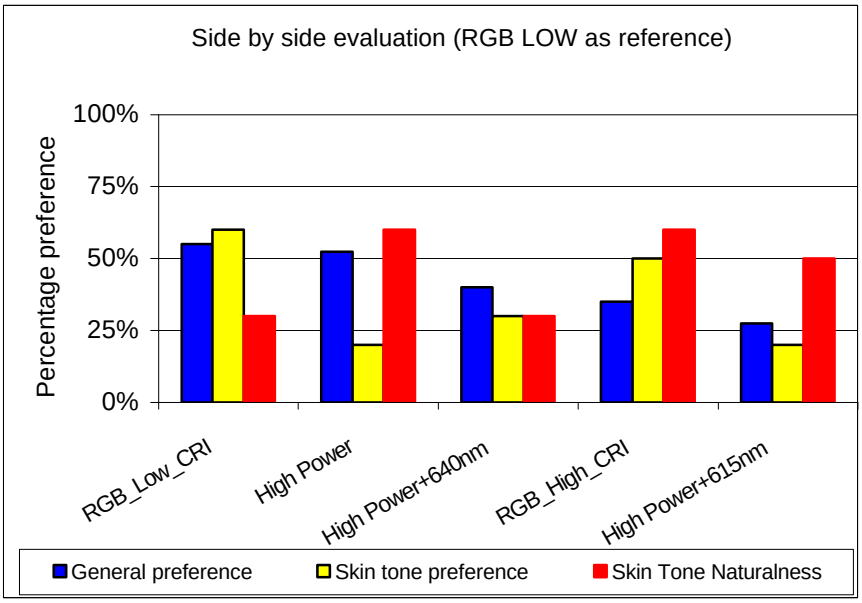

Fig. 24 Side-by-side Comparison with RGB Low CRI Reference Light Source

Table 5. Experimental Light Source Characteristics on the Scene

Light Sources	CCT	CRI	x	y	illuminance (fc)
High Power LED	5123	85	0.3401	0.3259	19.0
High Power LED +525 nm Green + 620nm Red	4436	88	0.3632	0.3662	19.2
High Power LED +525 nm Green + 640nm Red	4367	86	0.3656	0.3670	18.9
RGB mixed Low_CRI	4392	24	0.3647	0.3667	18.8
RGB mixed High_CRI	4532	64	0.3605	0.3673	18.8
Halogen Reference	2835	98	0.453	0.415	18.9
RGB_Low_CRI reference	4269	23	0.368	0.366	19.4

Table 6. General Preference Rating Bonferroni Paired t-Statistic Result

Lamp	RGB_Low_CRI	RGB_High_CRI	High Power+640nm	High Power+615nm	Halogen	High Power
Mean rating	5.1	4.9	4.5	4.1	3.5	3.3
RGB_Low_CRI		**no**	**no**	*	***	***
RGB_High_CRI			**no**	*	*	***
High Power+640nm				**no**	*	*
High Power+615nm					**no**	**no**
Halogen						**no**
High Power						

Table 7. Skin Tone Preference Rating Bonferroni Paired t-Statistic Result

Lamp	RGB_Low_CRI	RGB_High_CRI	High Power +640nm	Halogen_Ref	High Power +615nm	High Power
Mean rating	5.1	4.6	3.9	3.9	3.8	3.4
RGB_Low_CRI		no	*	*	*	*
RGB_High_CRI			no	*	*	*
High Power+640nm				no	no	*
Halogen_Ref					no	no
High Power+615nm						no
High Power						

R.5 Commercial LED Product Evaluations

In general, system integrators package LED arrays differently and they may chose to drive them differently. Therefore, the proposed test will evaluate the above-mentioned products at two different temperatures and two different operating currents. Figure 25 illustrates the expected relative light output as function of time for the different LEDs. In this figure, I1 and I2 represent the drive current and T1 and T2 represent the temperature.

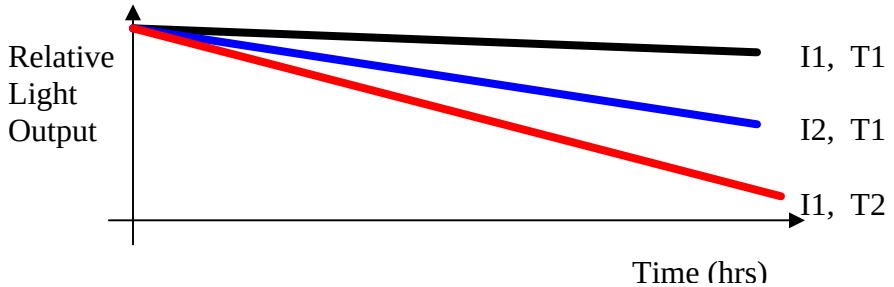

Fig. 25 Relative light output as a function of time.

The proposed experiment will allow us to investigate the amount of excess degrading due to drive current and the amount due to temperature increase. Prior to starting the life test each LED array (or the LED) will be measured for light output, power consumption and color (CCT, CIE x,y, and CCT). Then at regular intervals during the life test (say every 1000 hours) these parameters will be measured to see how power consumption and color varies over time.

The experimental apparatus is presently being designed. The proposed setup includes a wall of 20 - 30 chambers, approximately 10” square each. Each chamber contains an array of LED light sources, a temperature sensor, light sensor, and a heating coil to vary the temperature in each of the 20 chambers.

Some LEDs will be tested at room temperature (25 °C), others at higher temperatures. All of the data from the different chambers will be fed into a Data Acquisition Switch Unit and then to a computer for data analysis. As of this report, a prototype of one of the 20 chambers was built and tested. The data acquisition equipment is ordered, and the other components, such as temperature and light sensors, have

been selected and are being tested individually to evaluate their performance before completing the full order for the chambers.

The work will progress throughout this year and next year until the LEDs are tested for at least 10,000 hours. We hope to have the initial bath of LEDs started by the beginning of July 2002.

R.6 Development of Optical Designs For Next-generation Solid-State Lighting Fixtures

Multiple distribution types such as direct, semi direct, and indirect distributions, and fixture positions were analyzed for a conference room of size 10' X 10' X 8', to identify the best distribution type to obtain illuminance levels for the task. This analysis was done using Lightscape software. The distribution types are shown in Fig. 26 below.

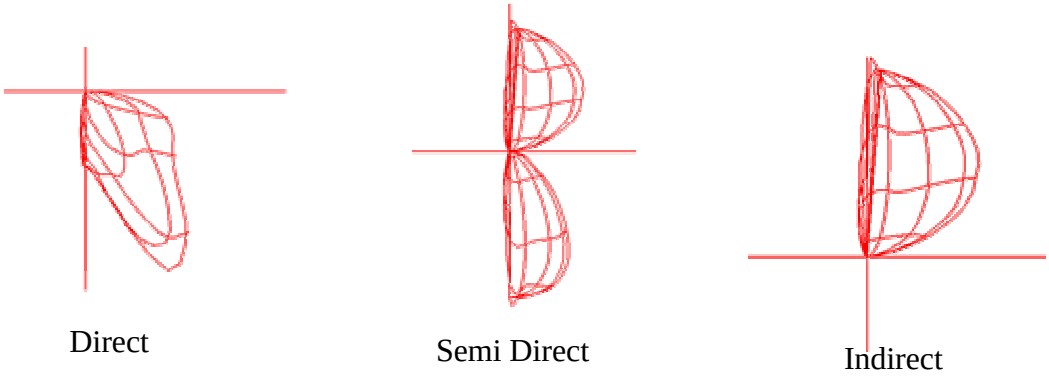

Fig. 26. Direct, semi-direct, and indirect beam distributions.

Room lighting can be achieved by placing the lighting fixtures in a variety of locations. Modeling of different approaches included placing each of four fixtures at the location of crown molding centered on each wall. In this initial evaluation two fixtures (total of 1500 lumens) that provided direct and indirect beam distributions were used and the respective table, wall, and floor illuminance distributions were obtained. The illuminance values on the table were around 500 lux, walls were around 300 lux, and the floor was around 300 lux. In addition the uniformity was within 30%.

Laser sources

Four laser diode sources are being considered and modeled for the project including a red focusable laser pointer, a green laser pointer, a red laser line generator, a simple laser diode, and a laser diode array. An example of the model for the laser pointer is given in Figs. 27 and 28. Figure 27 represents the model from a number of viewpoints. Figure 28 shows a line chart and a raster chart of the output on the receiver plane.

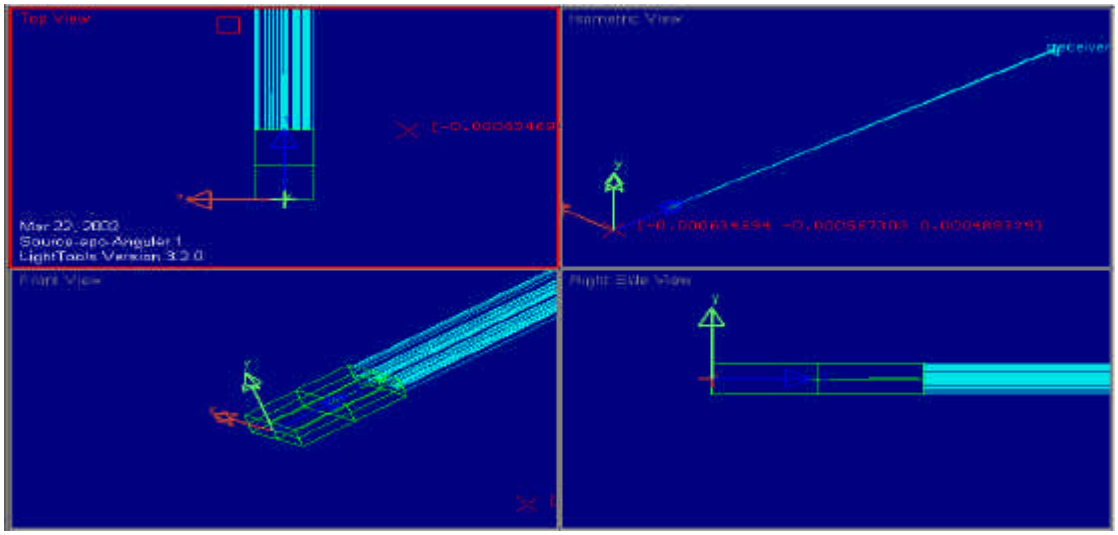

Fig. 27. Laser pointer source model

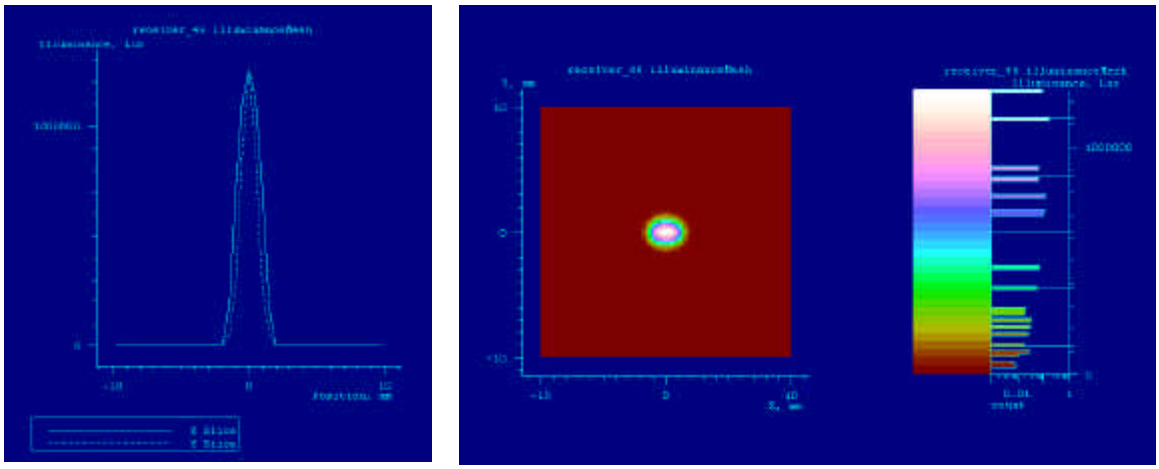

Fig. 28. Line chart and raster chart for laser pointer source model

Optical Modeling

Four approaches are being considered to determine the most appropriate path to create the luminaires for general illumination. The four approaches include transmissive optics, reflective optics, waveguide optics, and non-imaging optical solutions. Examples of the types of optical solutions that may be used are shown in Fig. 29.

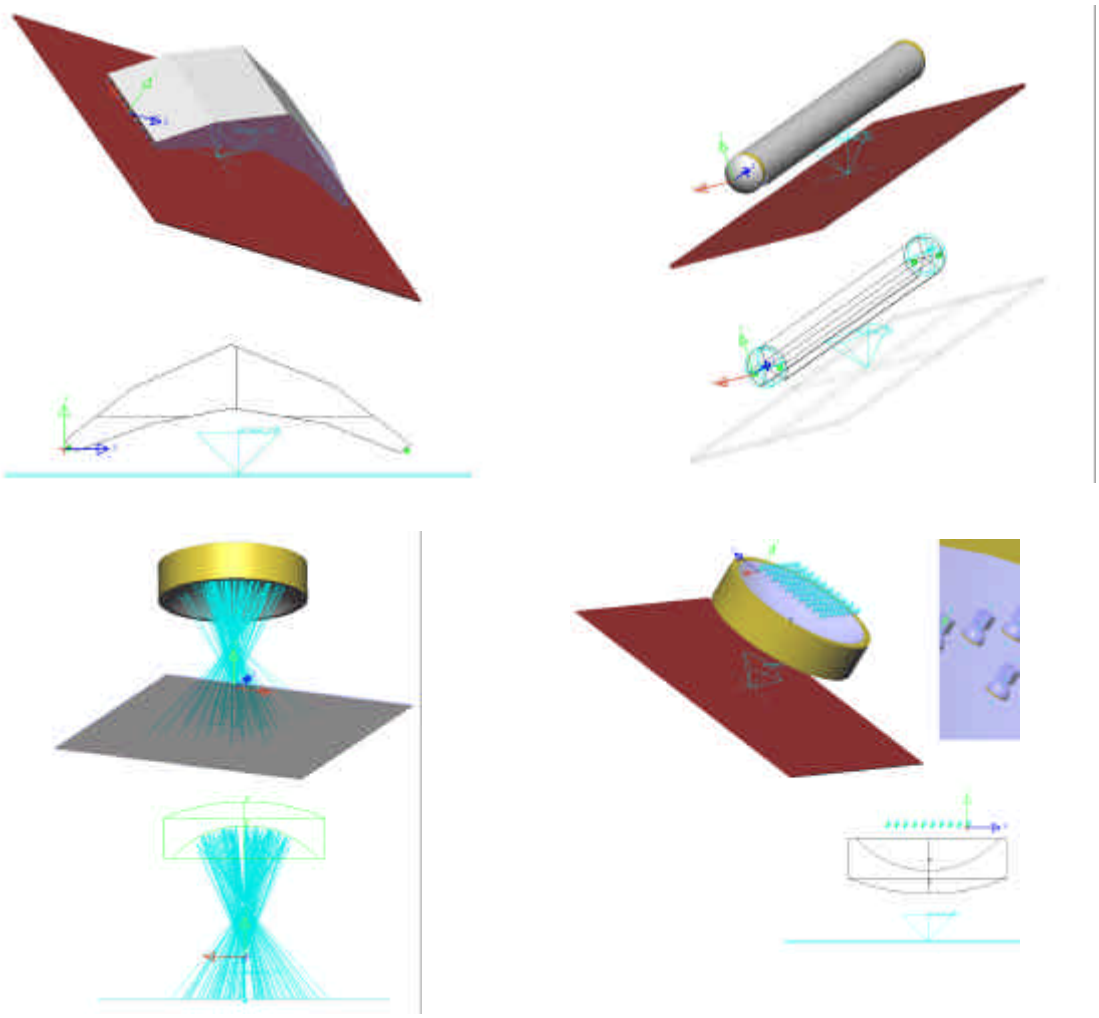

Fig. 29. Examples of conceptual designs for reflective, waveguide, and transmissive optical solutions for general illumination.

There are an endless number of concepts in each of these categories that could be considered. In order to reach a decision on a prototype for the first phase of this project, it was necessary to select one or two designs from these approaches. Transmissive optics and waveguide optics were chosen for this first phase. The goal of the optical design process was to determine what properties of the optics were most important to optimize efficiency and uniformity.

Waveguide Optics

An example of the waveguide approaches taken are shown in Fig. 30. The surface properties for the top surface of the cylindrical rod and for the sides of the square rod were varied to optimize efficiency and uniformity. Based on the modeling, a lambertian surface provides the most uniform illuminance on the receiving plane. In addition to surface properties, coupling the diverging laser source into the waveguide using total internal reflection (TIR) to reduce losses out of the bottom of the waveguide was performed. In addition, to enhance the TIR reflections, an angled back surface, a saw-tooth film bottom, and a saw tooth top are being considered. Finally, multiple sources and the placement of the sources at either or both ends of the optics is being considered.

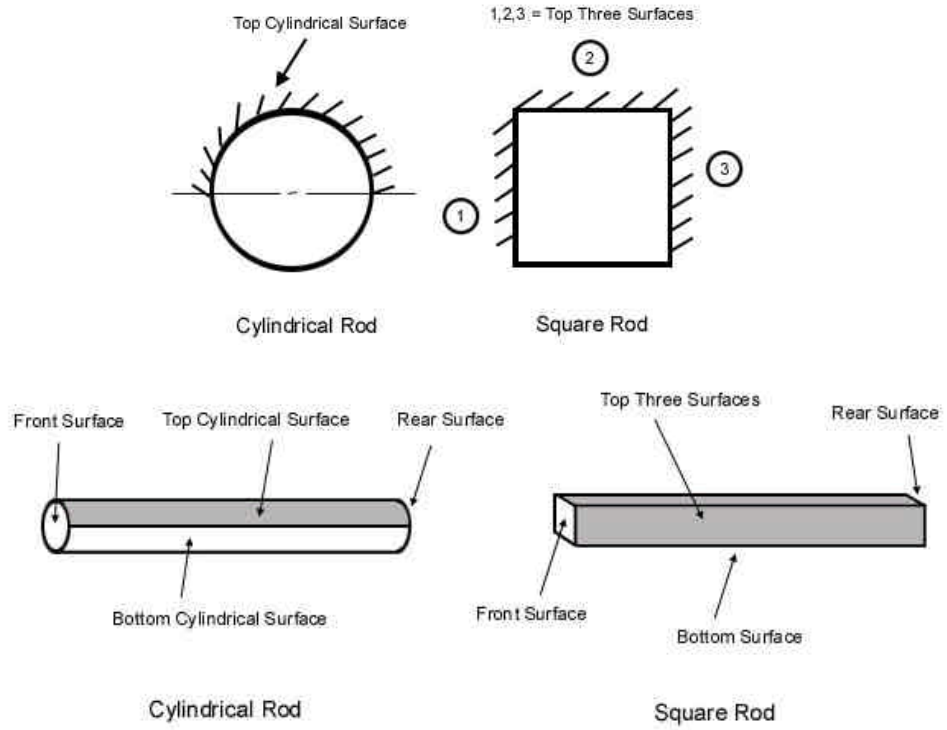

Fig. 30. Cylinder rod and square rod waveguide optics

A systematic analysis of the of the surface properties of the linear wave guide was made to understand what factors contributed to the uniformity of illuminance and efficacy. Table 8 lists the properties of the source, the waveguide optic, and the receiver used in the cylindrical rod simulation. Table 9 shows the results of the simulation. The results show that having a lambertian top surface provides the highest efficiency.

Table 8. Source, Optic, and Receiver Properties used in the Cylindrical Rod Simulation.

Part Name	Parameters	Values
Source	Type	37 deg. Line Generator
	Output Aperture	Front
	Diameter	9 (mm)
Rod	Material	n=1.59, V=30 (Fictitious)
	Surface Optical Properties	Cyl. Top = TIR (trans.=1.0) / Reflect(Ref.=1.0) / Lambertian Scatter
		Cyl. Bottom = TIR (trans.=1.0)
		Front = TIR (trans.=1.0)
		Rear = TIR (trans.=1.0) / Reflect(Ref.=1.0) / Lambertian Scatter
	Diameter	18 (mm)
	Length	300 (mm)
Receiver	Material	Aluminum_user
	Surface Optical Properties	Mechanical, Ref.=0.0, Trans.=0.0
	Type	Surface
	Receiver Distance	150 (mm)
	Receiver Plane Dimension	500*200 (mm)
	Mesh Resolution for Illuminance/color	5*5
Rays		10,000

Table 9. Results for Cylindrical Rod Simulation.

Condition No.	Cylindrical Top Surface	Rear Surface	Output Rays
1	Clear	Clear	No Rays from Bottom
2	Clear	Reflect	No Rays from Bottom
3	Clear	Lambertian	Rays Sample=**797**
4	Reflect	Clear	No Rays from Bottom
5	Reflect	Reflect	No Rays from Bottom
6	Reflect	Lambertian	Rays Sample=**1450**
7	Lambertian	Clear	Rays Sample=**3656**
8	Lambertian	Reflect	Rays Sample=**4525**
9	Lambertian	Lambertian	Rays Sample=**5057**

Table 10 shows the properties of the source, the waveguide optic, and the receiver used in the square rod simulation. Table 11 shows the results of the simulation. Again, the results show that having a lambertian top surface provides the highest efficiency.

Table 10. Source, Optic, and Receiver Properties used in the Square Rod Simulation.

Part Name	Parameters	Values
Source	Type	37 deg. Line Generator
	Output Aperture	Front
	Diameter	9 (mm)
Rod	Material	n=1.59, V=30 (Fictitious)
	Surface Optical Properties	Top Three = TIR (trans.=1.0) / Reflect(Ref.=1.0) / Lambertian Scatter
		Bottom = TIR (trans.=1.0)
		Front = TIR (trans.=1.0)
		Rear = TIR (trans.=1.0) / Reflect(Ref.=1.0) / Lambertian Scatter
	Width/Height	18/18 (mm)
	Length	300 (mm)
Receiver	Material	Aluminum_user
	Surface Optical Properties	Mechanical, Ref.=0.0, Trans.=0.0
	Type	Surface
	Receiver Distance	150 (mm)
	Receiver Plane Dimension	500*200 (mm)
	Mesh Resolution for Illuminance/color	5*5
Rays		10,000

Table 11. Results for Square Rod Simulation.

Condition No.	Top Three Surfaces	Rear Surface	Output Rays
1	Clear	Clear	No Rays from Bottom
2	Clear	Reflect	No Rays from Bottom
3	Clear	Lambertian	Rays Sample=**574**
4	Reflect	Clear	No Rays from Bottom
5	Reflect	Reflect	No Rays from Bottom
6	Reflect	Lambertian	Rays Sample=**773**
7	Lambertian	Clear	Rays Sample=**3400**
8	Lambertian	Reflect	Rays Sample=**4224**
9	Lambertian	Lambertian	Rays Sample=**5019**

Transmissive Optics

The transmissive approach being employed uses an array of laser diodes, each with a lens to increase the divergence of the beam. The array of laser diodes and accompanying lenses is followed by a large fennel lens to spread the beam a final time. The optical modeling of the transmissive system is shown in Fig. 31.

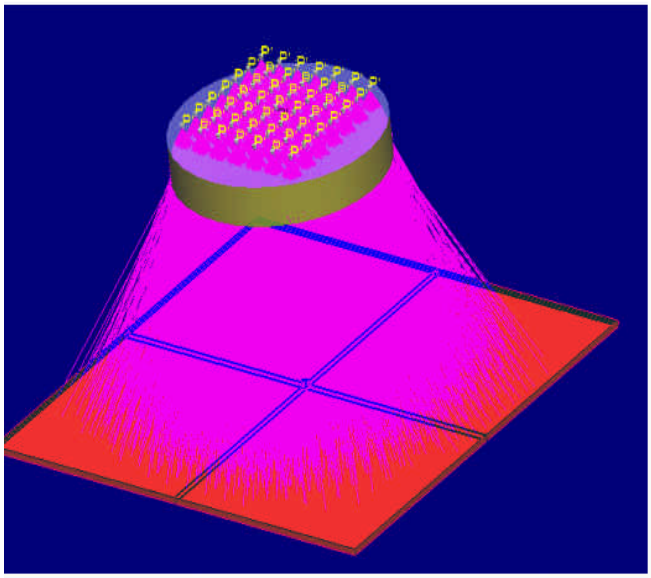

Laser Diode Array with Fresnel Lens

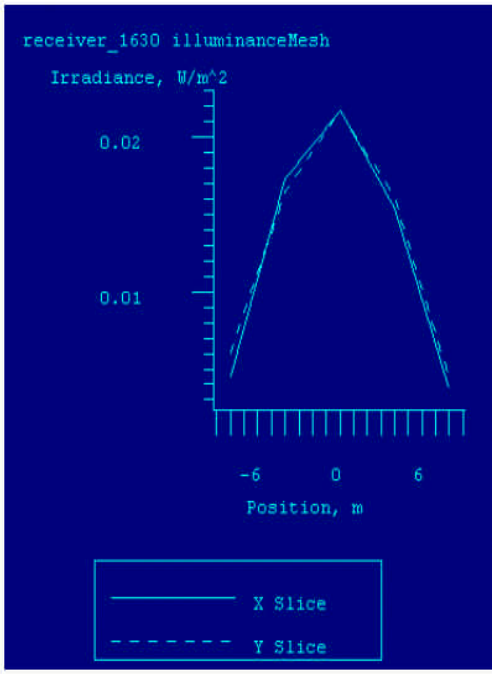

Illuminance line chart

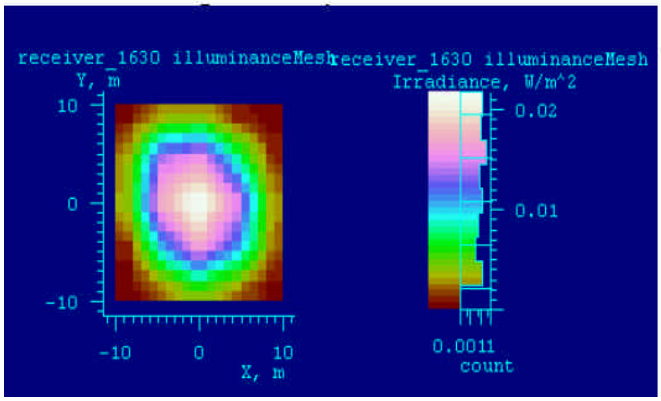

Raster image

Fig. 31. Transmissive optical model showing a picture of the model, a line chart and a raster chart of the illuminance

Next steps include finalizing the waveguide and transmission optical designs, ordering prototype optics, building the mock-up of the conference room, and testing the light levels to compare measured and calculated performance.

R.7 Development of suitable epoxy materials for packaging solid-state devices

The primary concern with the new epoxy mixtures of epoxy monomers with various polymers was to determine whether the epoxy curing reaction could be carried out in a similar manner as when no polymer additives are added. Preliminary studies have shown definitively that this is indeed the case. Kinetic studies were carried out using Real-time infrared spectroscopy (RTIR). Using this technique we are able to follow the course of the very rapid polymerization in real time while simultaneously

irradiating the sample with UV light. An example of the results of one of these experiments is shown in Fig. 32.

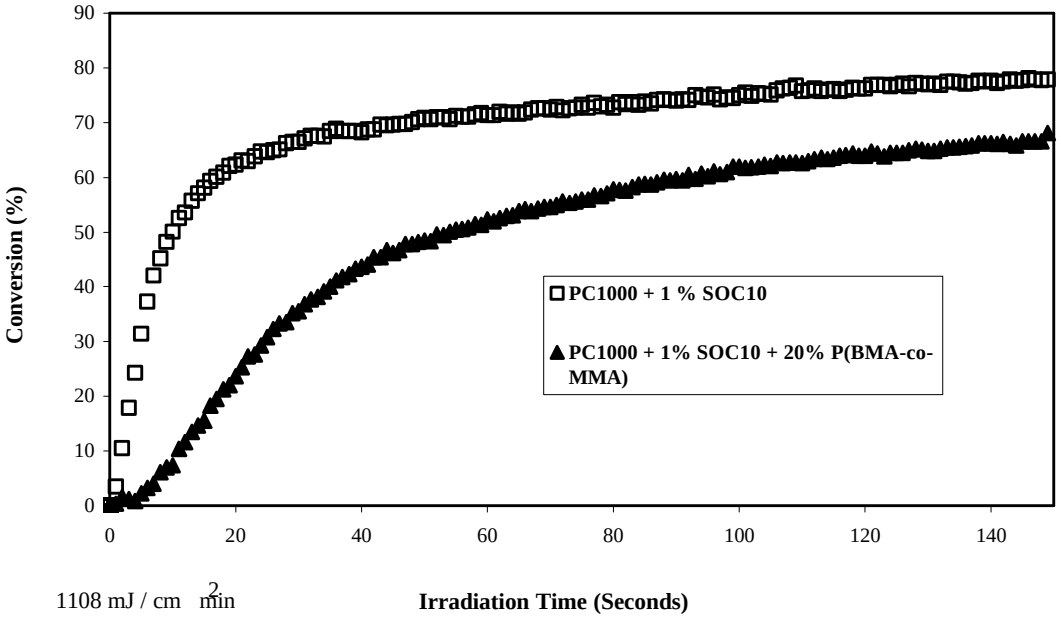

Fig. 32. RTIR study of the polymerization of PC1000 in the presence of SOC1O and in the presence and absence of 20% by weight of a poly(butyl methacrylate-methylmethacrylate) copolymer.

As may be noted in Fig. 32, the polymerization rate is reduced somewhat by the addition of the polymer. This is expected since the monomer has been diluted by the addition of 20 wt% of an inert polymer. It is particularly interesting to note that the polymerization still proceeds rapidly in the presence of the copolymer and that the polymerization of PC1000 proceeds to high conversion.

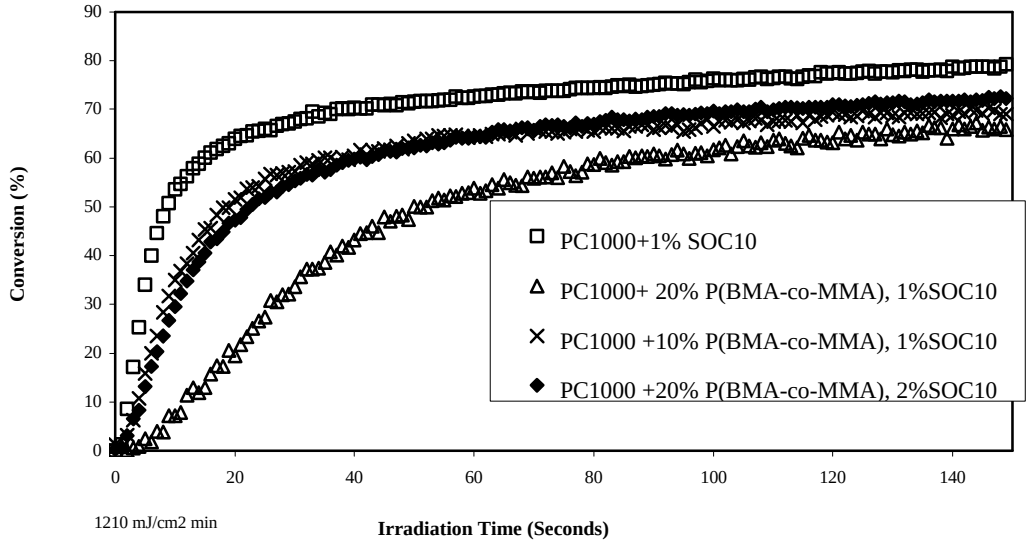

Fig. 33. Effect of the addition of 10% and 20% of Poly(BMA-co-MMA) on the polymerization of PC1000 with 1% and 2% of SOC10 as the photoinitiator.

The polymerization of PC1000 was reexamined as a function of different concentrations of the copolymer. It can be seen in Fig. 33 that increasing the concentration of the copolymer produces a

corresponding decrease in the polymerization rate. We have also attempted to determine whether the decrease in polymerization rate can be compensated by increasing the photoinitiator (SOC10) concentration. Considerable recovery of the rate can be achieved with compositions containing 20% copolymer by increasing the SOC12 concentration from 1% to 2%. At the same time, it is not possible to achieve rates comparable to those obtained with pure PC1000.

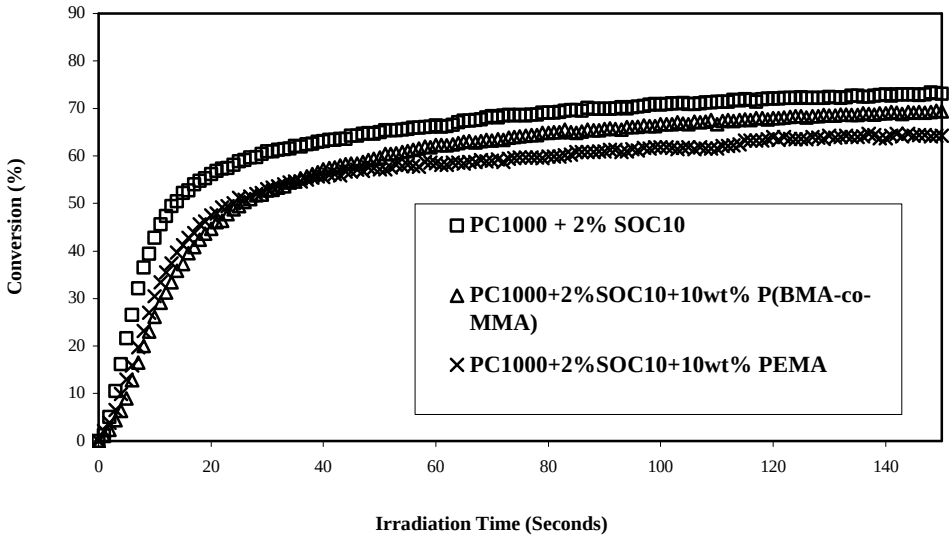

Fig. 34. RTIR Comparison of the photopolymerization rates of PC1000 in the presence of poly(BMA-co-MMA) and with poly(EMA).

Figure 34 shows a comparison of the UV induced polymerization of PC1000 in the presence of 10% poly(BMA-co-MMA) with the same monomer in the presence of 10% poly(ethylmethacrylate) (poly(EMA)). The methacrylate polymers have nearly identical UV curing response. This was predicted since the UV absorption spectra of the respective two polymers is nearly the same. We expect that it should be possible to use these and other acrylate and methacrylate polymers and copolymers to modify the mechanical and thermal properties of the epoxy matrix.

Disc samples of the UV cured PC1000 as well as PC1000 modified with the methacrylate polymers were prepared. These are colorless materials. Cured PC1000 is totally transparent and glasslike in appearance. Some of the modified samples showed haziness due to phase separation. It is believed that this problem can be overcome by increasing the light intensity to increase the cure rate.

In the next research period, continuation of the investigation of the UV induced polymerizations will be pursued. This will be carried out using the other two epoxy monomers described in this report. The use of other types of modifying polymers will also be pursued. In addition, we will begin to examine the thermal behavior (yellowness and thermal decomposition) of these materials. The first task will be to set up some protocols and methods to monitor these parameters.

CONCLUSIONS

As detailed in the Results section, we have made significant progress in the areas of VCSEL and UV LED development, as well as lighting and packaging design. We have refined the process of VCSEL device layer growth and processing to the point where we have obtained pulsed ~400 nm resonant-cavity LEDs, an important intermediate step to obtaining the ultimate goal of lasing. In particular, our use of indium tin oxide (ITO) top contacts, Ta_2O_5/SiO_2 dielectric mirror stacks, flip-chip bonding onto an AlN submount, and removal of sapphire substrate have all been shown to be important in the development of VCSEL structures. We have also found Al implanting to be useful in current confinement, although the problem of non-radiative defect formation during this process must be further investigated and ultimately minimized. A future key development will be the growth of VCSEL structures on laterally overgrown templates or 'bulk' free-standing GaN, both of which have low extended defect densities.

Our work on solid-state lighting design has focused on human factors experiments, evaluation of optimal lighting conditions in various scenarios, lighting fixture (luminaire) design, and UV-tolerant epoxy compositions. We have developed specifications for some of the key parameters for solid-state lighting systems by identifying three key tasks: First is a luminous flux requirement matrix for various lighting applications, which will aid us to identify the potential application once the light source is developed. The second is identifying an optimum spectral power distribution for the light source, so that it will be acceptable to human subjects. The third is benchmarking the performance characteristics of currently available commercial LEDs so that when we develop new light sources we can compare their performance against these commercial products. In the process of developing novel luminaire designs, we have considered luminaire arrangement geometry for a 'typical' room, the use of laser sources, and overall optical design (including transmissive optics, reflective optics, waveguide optics, and non-imaging optical solutions). Lastly, the important issue of encapsulating epoxy composition is under development, since currently available epoxies will likely not perform well under the high-power UV excitation from the AlGaN-based devices that are the goal of this project.